A Field Study of the Effect of Wall Mass on the Heating and Cooling Loads of Residential Buildings

(aka Log Home Report)

by

D.M. Burch, W.E. Remmert, D.F. Krintz, and C.S. Barnes

National Bureau of Standards
Washington, D.C. 20234

Proceedings of the Building Thermal Mass Seminar
Knoxville, TN; 6/2-3/82
Oak Ridge National Laboratory
Oak Ridge, TN

A FIELD STUDY OF THE EFFECT OF WALL MASS ON THE HEATING AND COOLING LOADS OF RESIDENTIAL BUILDINGS

D. M. Burch, W. E. Remmert, D. F. Krintz, and C. S. Barnes

National Bureau of Standards
Washington, D.C. 20234

ABSTRACT

Six test buildings were extensively instrumented for measuring heating and cooling loads, wall heat transmission, and indoor temperature and humidity. During these measurements, the effect of wall mass on the heating and cooling loads was observed. These buildings were exposed to a winter heating season, an intermediate heating season, and a summer cooling season.

The test buildings were 20 x 20 ft (6.1 x 6.1 m) one room buildings constructed at Gaithersburg, Maryland. These buildings had the same floor plan and orientation. They were identical, except for the wall construction, which was as follows: insulated lightweight wood frame; uninsulated lightweight wood frame; insulated masonry with outside mass; uninsulated masonry; log; and insulated masonry with inside mass. The insulated buildings including the log building were designed to have walls of approximately equivalent steady-state thermal resistance; the uninsulated buildings also were designed to have walls of approximately equivalent steady-state thermal resistance.

No reductions in heating energy attributable to wall mass were observed during the winter heating season, when the buildings typically did not float (i.e., some heating energy was supplied each hour). However, during the intermediate heating season and the summer cooling season, when the buildings floated during a portion of the day (i.e., no heating or cooling load occurred during a portion of the day and the indoor temperature rose above, or fell below the indoor set temperature), significant reductions in load attributable to wall mass were observed. Wall mass was observed to have a larger effect when it was placed inside the wall insulation as opposed to outside the wall insulation.

Key Words: thermal mass; wall heat transmission; residential energy consumption; and envelope heat transfer.

Proceedings of the Building Thermal Mass Seminar, Knoxville, TN; 6/2-3/82, ORNL, Oak Ridge, TN

NOMENCLATURE

A, B, C, and D = constants

A_f = surface area of floor, ft^2

A_i = surface area of i-th building component, ft^2

A_w = surface area of south-facing windows, ft^2

c_i = initial concentration of tracer gas

c_f = final concentration of tracer gas

C_p = specific heat of air, Btu/lb·°F

h_{fg} = latent heat of vaporization, Btu/lb

H = daily-average solar radiation incident on a south-facing vertical surface, $Btu/h \cdot ft^2$

I = rate of air infiltration, h^{-1}

K = envelope heat-transfer coefficient, Btu/h·°F

m = mass rate of flow, lb/h

P = period of time, h

P_e = electric power, W

Q_c = cumulative cooling load, Btu

Q_e = daily electric load for a building, Btu/h

Q_f = slab heat-loss rate to earth, Btu/h

Q_h = heating load, Btu/h

Q_i = internal heat release rate, Btu/h

R = thermal resistance, $h \cdot ft^2 \cdot °F/Btu$

T_b = balance point temperature, °F

T_i = average indoor air temperature, °F

T_g = earth temperature 20 in. (0.51 m) below the center top surface of floor slab, °F

T_o = average outdoor air temperature, °F

t = time or elapsed time, h

ΔT = temperature difference, °F

U = thermal transmittance, $Btu/h \cdot ft^2 \cdot °F$

U_f = thermal transmittance of floor slab, $Btu/h \cdot ft^2 \cdot °F$

U_i = thermal transmittance of i-th component, $Btu/h \cdot ft^2 \cdot °F$

v = rate of which air enters or leaves an enclosure, ft^3/h

V = mean observed wind speed, mph

$\forall$ = volume of enclosure, ft^3

β = solar loading coefficient, ft^2

τ = solar transmission coefficient for window

ρ = density of air, lb/ft^3

1. INTRODUCTION

Energy consumption for residential space heating and space cooling represents about 12 percent of the total energy required in the United States. With the advent of fuel shortages which have produced spiraling energy costs, much attention has been focused on strategies for reducing energy consumption in residential buildings. A strategy, which is the subject of this paper, deals with the effect of wall mass on the heating and cooling loads of residential buildings.

The effect of wall mass may be illustrated by considering a residential building exposed to an outdoor condition for which the outdoor temperature approaches the balance point (float zone) for the building. If the heating/cooling plant is turned off, the indoor temperature will fluctuate in response to the outdoor diurnal temperature variation. The building envelope will provide a reduction in the amplitude of the diurnal outdoor temperature waveform. Consider a masonry and comparable wood-frame residence having equivalent steady-state thermal resistance in the components of their envelopes. The amplitude reduction will be considerably greater for the masonry residence than for the wood-frame residence, owing to large heat capacity of the masonry material. Therefore, if high and low thermostat set points are established for space cooling and space heating, the masonry building will have considerably smaller indoor temperature excursions above and below the high and low set points, thereby causing its heating and cooling energy to be smaller than that for the wood-frame residence.

To date, the effect of wall mass on the heating and cooling energy consumptions of residential buildings has been investigated exclusively using computer programs. These studies [1-4] have shown that wall mass has a small effect on heating and cooling energy consumption. For instance, the results of the Peterson study [1] indicated that the reduction in heating energy requirements between a masonry residence and a comparable wood-frame residence ranged from 0.5 percent in northern U.S. climates to 17.6 percent in southern U.S. climates. Similarly, the percent difference in summer cooling requirements between masonry and comparable wood-frame residences [effect of wall mass on cooling energy] has been shown to be greater in climates having small cooling requirements (i.e., northern locations) [1,3]. Wall mass has been shown to be more effective when it is placed inside of wall insulation [3-5].

The objective of the present study is to experimentally investigate the effect of wall mass on space heating and space cooling loads of residential buildings. The study is presented herein.

2. DESCRIPTION OF TEST BUILDINGS

Six 20 ft (6.1 m) wide and 20 ft (6.1 m) long one-room test buildings with a 7-1/2-ft (2.3 m) high ceiling were constructed outdoors at the National Bureau of Standards located at Gaithersburg, Maryland.[1/] A photograph of one of the test buildings is given in Fig. 1. These buildings had the same floor plan and orientation. They were identical, except for the wall construction, which was as follows:

No. 1. insulated lightweight wood frame;
No. 2. uninsulated lightweight wood frame;

1/ Dimensions are inside dimensions.

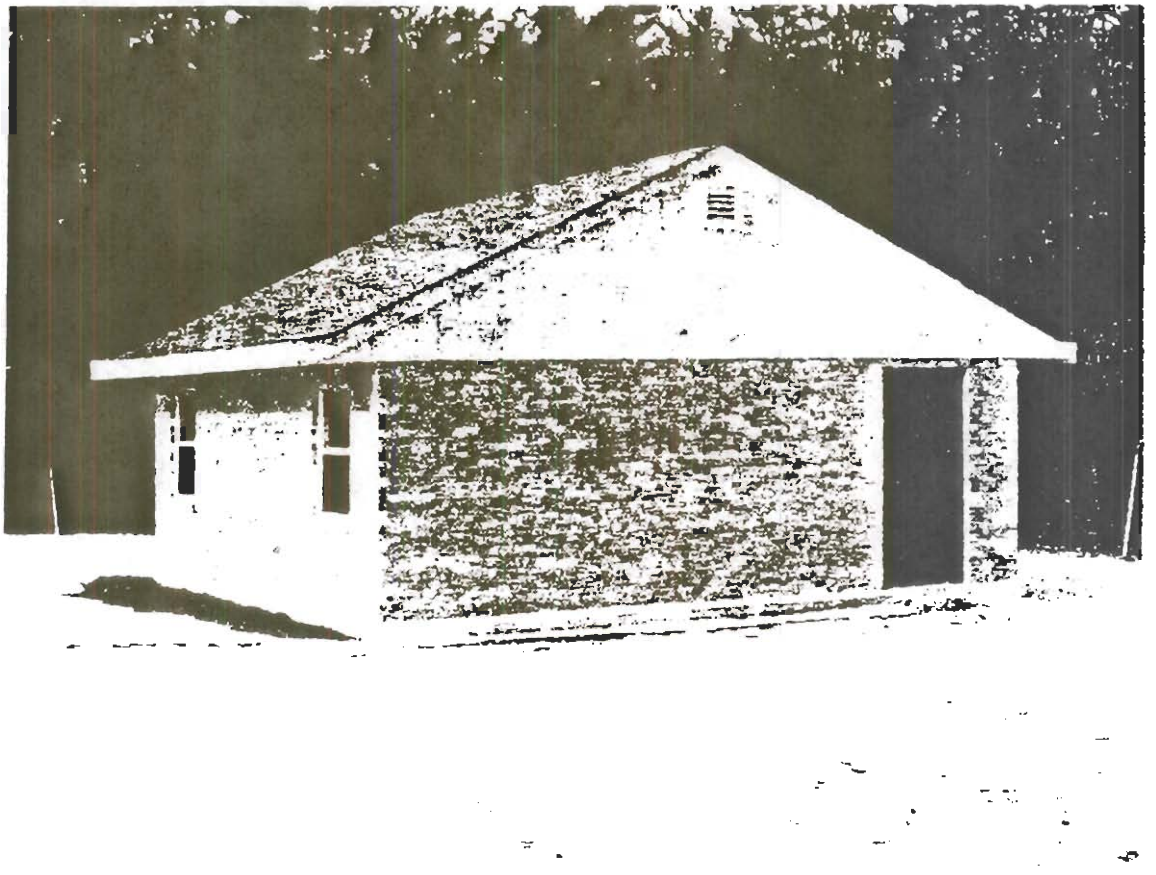

Fig. 1. Photograph of one of the test buildings.

No. 3. insulated masonry (outside mass);

No. 4. uninsulated masonry;

No. 5. log; and

No. 6. insulated masonry (inside mass).

A detailed description of the walls of the test buildings is given in Table 1. The characteristics for walls of the test buildings are given in table 2. The steady-state thermal resistances of the walls of Building Nos. 1, 3, 5, and 6 were designed to be approximately equivalent. Similarly, the steady-state thermal resistances of the

Table 1

Construction Details of Walls

No. 1 Insulated Lightweight Wood Frame

0.5-in. gypsum board
0.002-in. polyethylene film
2 x 4 studs place 16 in. o.c. with R-11 blanket insulation installed between the studs
5/8-in. exterior plywood

No. 2 Uninsulated Lightweight Wood Frame

(same as No. 1, except no insulation)

No. 3 Insulated Masonry (Outside Mass)

0.5-in. gypsum board
0.002-in. polyethylene film
2-in thick extruded polystyrene insulation placed between 1-1/2-in. wide wood furring strips placed 24 in. o.c.
1/4-in. air space
4-in. 2-core hollow concrete block at 105 lb/ft^3
4-in. face brick

No. 4 Uninsulated Masonry

0.5-in. gypsum board
0.002-in. polyethylene film
3/4-in. air space created by 2 x 3/4 in. furring strips placed 16 in. o.c.
8-in. 2-core hollow concrete block at 105 lb/ft^3

No. 5 Log

7-in. square lodge-pole-pine logs held together with tongue and grove locking system

No. 6 Insulated Masonry (Inside Mass)

0.5-in. plaster
8-in. 2-core hollow concrete block at 105 lb/ft^3
3-1/2-in. perlite insulation in cavity
4-in. face brick

---

1 in. = 2.54 cm
1 ft = 0.305 m

walls of Building Nos. 2 and 4 were designed to be approximately equivalent. With the exception of Building No. 6, an effort was made to make the construction representative of current construction practices of the United States.

Identical electrical service including electrical receptacles, a light switch, a circuit breaker box, a fluorescent light fixture, and electric service lines run through conduits were installed at the interior surface of each test building.

Table 2

Characteristics of Walls for Test Buildings

Building	Wall Description	Thermal Resistance* $h \cdot ft^2 \cdot °F/Btu$	Weight lb/ft^2
1	Insulated Wood Frame	12.2	4.4
2	Uninsulated Wood Frame	3.6	4.2
3	Insulated Masonry (Outside Mass)	13.7	64.
4	Uninsulated Masonry	4.6	42.
5	Log	10.3	17.
6	Insulated Masonry (Inside Mass)	12.4	83.

* The thermal resistance values are based on guarded-hot-box measurements described in section 3.2 and include air films with thermal resistances of 0.68 $h \cdot ft^2 \cdot °F/Btu$ at inside surface and 0.40 $h \cdot ft^2 \cdot °F/Btu$ at outside surface.

The interior surfaces of the test buildings were painted with an off-white latex paint. The exterior surfaces of Building Nos. 1, 2, and 4 were painted with an exterior paint having approximately the same color as the exterior face brick of Building Nos. 3 and 6.

Two double-hung, insulating glass (double pane) windows were located on the south-facing walls and two on the north facing walls. Each window contained two glass panes separated 3/16 in. (0.48 cm) with carbon-dioxide gas filling the cavity. An exterior storm window was fitted to each window. The total window area was 43.8 ft^2 (4.07 m^2), or 11 percent of the floor area.

Each test building had a 19.5 ft^2 (1.81 m^2) hollow metal door on the east wall. The door cavities were filled with perlite insulation. Each test building contained a pitched roof with an attic space ventilated with soffit and gable vents. The ventilation opening was consistent with the HUD Minimum Property Standard. Eleven inches of glass-fiber blanket insulation (R-34 (R-6.0 $m^2 \cdot K/W$)) was installed over the ceiling of each test building.

The edges of the concrete slab-on-grade floors were insulated with 1-in. (2.54 cm) thick polystyrene insulation at both the inner and outer surfaces of the footing (see concrete slab floor, foundation, and footing detail shown in Fig. 2).

Each test building was equipped with a centrally located 4.1 kW electric forced air heating plant equipped with a 13,000 Btu/h (3800 W)[1/] split vapor-compression air conditioning system. The evaporator coil was installed above the electric heating element. The compressor and condensor were located in an outdoor unit located at the center of the north wall of each test building.

1/ The cooling capacity of the air conditioning was rated by manufacture at suction temperature of 45°F (7.2°C) and suction pressure of 76.6 psig (3670 Pa) and an air temperature on condensor of 95°F (35°C).

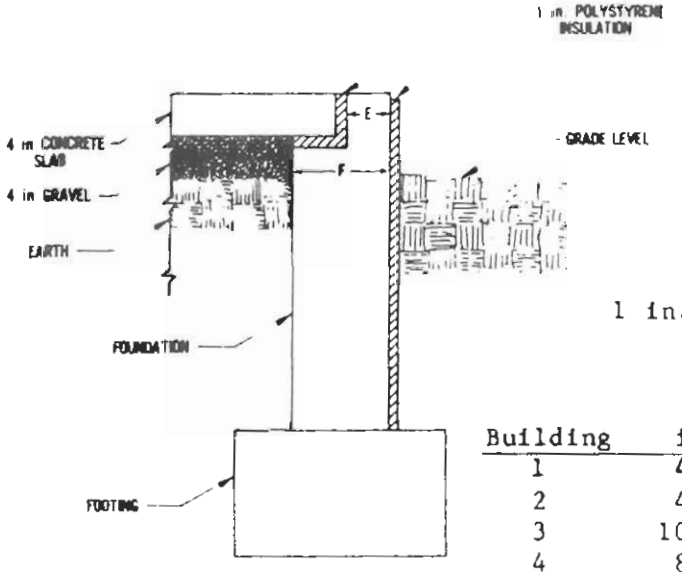

1 in. = 2.54 cm

Building	E in.	F in.
1	4	9
2	4	9
3	10 1/8	15 7/8
4	8 7/8	13 7/8
5	7	12
6	15 1/8	20 7/8

Fig. 2. Concrete slab floor, foundation, and footing detail.

3. HEAT-TRANSFER PROPERTIES

Detailed heat-transfer properties are given in the appendix. Heat-transfer properties pertinent to the analysis of the paper are presented herein.

3.1 Windows

The thermal transmittance of the window system was determined by developing heat balance equations for the three glass surfaces, and solving these equations simultaneously. Under both winter and summer conditions, the thermal transmittance was found to be 0.36 Btu/h•ft^2•°F (2.04 W/m^2•K). A framing factor of unity was used in the analysis.

The solar transmission coefficient (τ) for the south-facing window systems was measured using a reflectometer, giving a value of 0.61. This value was an average value for the upper and lower portions of the window. The lower portion of the windows contained an insect screen and the upper portions did not.

3.2 Walls

The steady-state thermal conductances of the walls for each building was predicted using the series resistance method. Studs and furring strips were treated as parallel heat flow paths. Predicted steady-state surface-to-surface thermal resistance values are presented in Table 3 along with corresponding measured values determined by guarded-hot-box measurements on 6 x 6 ft (2.4 x 2.4 m) wall specimens having identical construction as the walls of the test buildings. For the guarded-hot-box measurements, each wall specimen was sandwiched between a hot box maintained at approximate 70°F (21°C) and a cold box maintained at approximate 35°F (1.7°C) and permitted to reach thermal equilibrium. The resulting heat-transfer rate through a 48 x 32 in.

(1.2 x 0.81 m) metering section was measured. Based on separate measurements of homogeneous test specimens having known thermal properties,

Table 3

Comparison of Thermal Resistances[1/] Measured with a Guarded-Hot-Box Apparatus to Corresponding Predicted Values

	Surface Temp., °F			Thermal Resistance $h \cdot ft^2 \cdot °F/Btu$		$\frac{M - P}{M}$[2/]
Building	Hot Side	Cold Side	Mean	Measured	Predicted	% Diff
1	72.6	34.6	53.6	11.14	11.88	- 6.6
2	71.4	40.4	55.9	2.52	2.36	+ 6.3
3	71.2	27.2	49.2	12.61	12.18	+ 3.4
4	74.9	38.1	56.5	3.55	2.99	+15.8
5	81.1	40.6	60.9	9.25	9.83	- 6.3
6	73.6	26.4	50.0	11.34	11.58	- 2.1

1/ These are surface-to-surface thermal resistance values. The air flow rate across the warm-side and cold-side surfaces were 0.7 (0.3) and 0.4 mph (0.2 m/s), respectively.

2/ M and P denote measured and predicted values of thermal resistance.

$C = 5/9(F - 32)$

$1\ h \cdot ft^2 \cdot °F/Btu = 0.176\ m^2 \cdot K/W$

the measurement precision of the guarded-hot-box apparatus was determined to be better than 5 percent.

The wall thermal transmittance values used in the calculation of envelope heat-transfer coefficients were obtained from the relation:

$$U = \frac{1}{1/h_i + R + 1/h_o} \qquad (1)$$

where h_i = inside surface heat-transfer coefficient, 1.46 $Btu/h \cdot ft^2 \cdot °F$ (8.29 $W/m^2 \cdot K$)

R = surface-to-surface thermal resistance, $h \cdot ft^2 \cdot °F/Btu$; and

h_o = outside surface heat transfer coefficient, 2.5 $Btu/h \cdot ft^2 \cdot °F$.

The solar absorptances of the exterior walls were measured prior to the summer cooling measurements using a reflectometer and found to be 0.40, 0.40, 0.64, 0.38, 0.69, and 0.65 for Building Nos. 1, 2, 3, 4, 5 and 6, respectively. After the summer cooling measurements,[1/] the exterior walls of Building Nos. 1, 2, and 4 were painted with a paint system having approximately equivalent color as the exterior brick for Building Nos. 3 and 6. The solar absorptances were again measured prior to the winter heating measurements and found to be 0.62, 0.61, 0.58, 0.58, 0.78, and 0.55 for Building Nos. 1, 2, 3, 4, 5, and 6, respectively. The solar absorptance of the log wall appeared to depend upon the solar altitude, indicating that this surface was somewhat specular.

3.3 Doors

The same procedure as used for the walls (section 3.2) was used to predict the thermal transmittance of the door giving a value of 0.144 $Btu/h \cdot ft^2 \cdot °F$ (0.818 $W/m^2 \cdot K$).

3.4 Ceiling/Roof Combination

The thermal transmittance of the ceiling/roof combination was determined by performing a heat balance on the attic space and predicting an attic air temperature which was subsequently used to predict the ceiling heat transfer rate. This procedure showed that the thermal

---

1/ The winter heating measurements were actually carried out after the summer cooling measurements, but they are reported in reverse order in the paper.

transmittance of the ceiling/roof combination was essentially equal to that of the ceiling alone due to the fact that the ceiling was highly insulated (R-34 (R-6.0 $m^2 \cdot K/W$)). The effective thermal transmittance of the ceiling was found to be 0.0265 $Btu/h \cdot ft^2 \cdot °F$ (0.151 $W/m^2 \cdot K$).

3.5 Floor Slab

For the winter heating season with the floor slabs insulated, an analysis of the floor slab heat-flow meter data showed that the heat loss from the floor slab consisted of a uniform earth loss and an edge loss component. The following relation provided a good estimate of the earth loss (Q_f):

$$Q_f = U_f \cdot A_f \cdot (T_i - T_g) \qquad (2)$$

where U_f = steady-state transmittance of the floor, gravel, and 1 foot (0.305 m) of earth, $Btu/h \cdot ft^2 \cdot °F$;

A_f = surface area of floor, ft^2;

T_i = indoor air temperature, °F; and

T_g = earth temperature 20 in. (0.51 m) below the center of the floor surface, °F.

The conductance (U_f) at the center of the floor slab was calculated by the series resistance method and found to be 0.0714 $Btu/h \cdot ft^2 \cdot °F$ (0.406 $W/m^2 \cdot K$). It should be pointed out that the temperature 20 in. (0.51 m) below the edge of the floor slabs was considerably colder than that 20 in. (0.51 m) below the center of the floor surface.

The edge conductance of the insulated floor slab was estimated by the following procedure. A weekly average floor heat loss profile was obtained by time averaging hourly heat fluxes measured by the row of heat-flow meters installed across the floor slab. A uniform earth loss was estimated from eq. (2) and subtracted from this profile,

yielding an edge loss profile. This edge loss profile was subsequently integrated across the floor surface and divided by the average inside-to-outside temperature difference, giving an edge heat-transfer coefficient of 5.0 Btu/h•°F (2.6 W/K). The process of integrating the edge loss profile across the floor surface contained considerable uncertainty due to the lack of information concerning the edge loss at corners. Fortunately, the edge heat-transfer contributes only a small amount to the overall envelope heat loss.

3.6 Infiltration

Nine winter infiltration rates for each building were measured under a wide range of outdoor temperatures and wind speeds. The data obtained for each building was fitted to an equation of the form:

$$I = A + B \cdot \Delta T + C \cdot V^2 \qquad (3)$$

where ΔT = average observed inside-to-outside temperature difference, °F;

V = mean observed wind speed, mph; and

A, B, and C = coefficients determined from regression analysis procedure.

Mean air infiltration rates for each building for the 98-day winter heating season (see section 5) were predicted by the foregoing equation using the mean temperature difference and wind speed for the period of analysis.

The regression coefficients A, B, and C for eq. (3), the mean infiltration rates, and the residual standard deviations from the fitted equations are summarized in Table 4.

4. INSTRUMENTATION AND MEASUREMENT TECHNIQUE

4.1 Outdoor Weather Measurements

The wind speed and direction were measured with a rotating-cup anemometer and a potentiometer-type, wind-direction vane mounted onto a 25 ft (7.6 m) mast co-located with the test buildings. The outdoor temperature and humidity were measured with a thermocouple and

Table 4

Infiltration Measurements

Building	A h^{-1}	B $h^{-1}/°F$	C h^{-1}/mph^2	Mean[1/] Infil. Rate h^{-1}	Residual Standard Dev. h^{-1}
1	-.00134	.00274	.000340	.13	.022
2	+.0111	.00195	.000153	.078	.015
3	+.0219	.00237	.000267	.10	.040
4	-.00558	.00190	.000176	.060	.018
5	+.0143	.00350	.000229	.133[2/]	.027
6	+.0171	.00168	.000110	.074	.016

[1/] The mean infiltration rates were determined at a mean wind speed of 3.4 mph and a mean inside-to-outside temperature difference of 33.2°F.

[2/] The mean infiltration rate for Building No. 5 was large due to a crack at the west wall/ceiling interface that developed at the beginning of the 1982 winter season.

Dunmore-type relative humidity transducer mounted 1 ft (0.305 m) from the center of the north-facing wall of the Instrumentation Building. The hemispherical radiation incident on a south-facing vertical surface was measured with a pyranometer mounted 1 ft (0.305 m) above the ground and centered on the south-facing wall of Building No. 1.

Signals from the wind speed sensor and solar vertical pyranometer were integrated using analog integrators to obtain average hourly values. The instantaneous signals from the other weather transducers were inputted into a data acquisition system which recorded the signals at hourly intervals.

4.2 Energy Measurements

The total electrical energy utilized by each test building was measured using a watt-hour meter equipped with a demand metering device which generated a contact closure for each 3.60 W•h (13,000 J) consumed. The accuracy of the watt-hour meters as given by the manufacturer was 1/2 percent. The contact closures were totalized and recorded at hourly intervals. The watt-hour meters were also read manually at 1000 hours each work day. The heating load for each test building was determined by subtracting the constant internal load from the total electric energy consumption.

For the summer cooling energy measurements, the cumulative cooling load (Q_c) was determined from the relation:

$$Q_c = m \cdot C_p \cdot \int_0^P \Delta T \, dt + W \cdot h_{fg} \qquad (4)$$

where m = mass flow rate of air through cooling plant, lb/h;

C_p = specific heat of air, Btu/lb•°F;

ΔT = temperature drop of air upon passing through cooling plant, °F;

t = time, h;

W = mass of condensate collected during period P, lb;

h_{fg} = latent heat of vaporization of water, Btu/lb; and

P = period of time over which the blower of the cooling plant operates, h.

The first and second terms represent the sensible and latent portions of the cooling load, respectively.

The temperature drop (ΔT) was sensed with a 32-junction copper-constantan thermopile. Sixteen of the junctions were arranged in an equally-spaced grid network and mounted in the return plenum of the cooling plant; the other sixteen junctions were similarly arranged and mounted in the supply plenum.

The millivolt signal from each thermopile was fed into a switching circuit. When the blower of the cooling plant operated, the switching circuit applied the thermopile millivolt signal into an analog integrator. When the blower stopped; the switching circuit applied a short circuit across the input terminals of the analog integrator, thereby ceasing the integration.

The mass flow rate of air ($\dot{m}$) through the cooling plant was measured using an air-flow measuring device mounted in a long, straight return air duct. The air-flow measuring device consisted of a honeycomb air straightener followed by an array of pitot tubes for measuring the total pressure and an array of pressure ports around the perimeter for measuring the static pressure. The difference in pressure between these two arrays was sensed with a micro-manometer to give a reading of the velocity pressure from which the air speed was determined.

The foregoing sensible load measurement does not account for heat transfer at the exterior surface of the indoor unit. These heat gains should be small, since the exterior jacket of the cooling plant was insulated with R-11 (R-1.9 $m^2 \cdot K/W$) blanket insulation.

A special test was carried out to determine the accuracy of the sensible load measuring system. For this test, the electric heating plants were operated continuously until a steady condition was achieved.

The electric power to each heating plant was measured using the watt-hour meters. The electric power (P_e) delivered to the heating plant was also determined from the relation:

$$P_e = m \cdot C_p \cdot \Delta T \qquad (5)$$

where m = mass flow rate of air through the heating plant measured by the air flow measuring device, lb/h;

C_p = specific heat of air, Btu/lb·°F; and

ΔT = temperature drop across the heating plant measured with the thermopile, °F.

The agreement between the measured electric power and the electric power determined from eq. (5) was within 6 percent for the six sensible load measuring systems. Therefore, the uncertainty in the sensible load measuring system was $\pm$ 6 percent. Probably most of the error in the sensible load measurement is the uncertainty in the air speed measurement.

Condensate from the evaporator coil of each air conditioner was collected in a 7-1/2-in. (19 cm) diameter, 34-in. (0.86 m) high cylinder. Installed in the bottom of each cylinder was a pressure transducer which produced a D.C. signal proportional to the weight of water in the cylinder. The millivolt signal (i.e., the weight of water in the cylinder) was recorded at hourly intervals by the data acquisition system.

4.3 Wall Heat Transmission

The heat flow rate was measured at the center of each of the four walls of the test buildings. Heat-flow meters, consisting of a 2 x 2 in. (5.1 x 5.1 cm) wide and 1/8-in.-thick (0.64 mm) wafers containing an embedded thermopile, were spot glued at the inside wall surface. Heat-flow meters produce a D.C. signal proportional to the instantaneous heat-flow rate passing through the device. When studs or furring strips

were present, the heat-flow meters were installed midway between these structural members. Inside and outside surface thermocouples were installed in the immediate vicinity of the heat-flow meters. In addition, an inside air temperature thermocouple was mounted at this same location using a bracket extending 1 ft (0.205 mm) from the inside surface.

4.4 Indoor Temperature and Humidity

The indoor air temperature was measured with thermocouples mounted along two thermocouple strings installed 5 ft (1.5 m) from the center of the north- and south-facing walls of each test building. Air temperature thermocouples were located along each string at the following levels: 2 in. (5.1 cm), 1 ft (0.31 m), 2 ft (0.61 m), and 5 ft (1.5 m) above the floor and 2 in. (5.1 cm) below the ceiling.

The indoor relative humidity of each test building was measured with a Dunmore-type relative humidity transducer mounted at the 5 ft (1.5 m) level of the north thermocouple string.

4.5 Other Measurements

The attic air temperature was measured with copper-constantan thermocouples at three locations within the attic space of each test building. An umbrella-shaped metal radiation shield was installed about 1/2 in. (1.3 cm) above each thermocouple junction so that it would not sense heat from the hot roof above.

The earth temperature under each floor slab was measured with a copper-constantan thermocouple installed at the center and 20 in. (0.51 m) below the floor surface.

The top floor surface of Building No. 3 was instrumented with heat-flow meters. Heat-flow meters were spot glued at the following

locations along a center line connecting the north- and south-facing walls: 0.5 (0.15), 1.0 (0.30), 2.0 (0.61), 3.0 (0.91), and 4.0 ft (1.2 m) from north and south walls and at the center of the slab.

4.6 Data Acquisition

One-hundred-channel data acquisition systems were installed in Building Nos. 1, 3, and 5. Each system served the building it was located in and the even number building located across from it. Data was recorded on paper at hourly intervals.

4.7 Air Infiltration Measurements

To determine the rate of air exchange between a test building and the surroundings, the rate of disappearance of sulfur-hexafluoride (SF_6) tracer gas was measured. A small quantity of SF_6 was released using a hypodermic syringe over a small portable room fan. After mixing had occurred, bag samples of indoor air were drawn from each building through a tube which penetrated the wall. The concentration of SF_6 within each building was subsequently permitted to decay over about a 16-hour period, after which bag samples of the indoor air were again drawn from each building. During the measurement period, the wind speed was continuously integrated to give average hourly values and the inside-to-outside temperature difference was recorded at hourly intervals.

The rate of change of concentration of tracer gas caused by infiltration was treated as a first-order exponential process expressed by the relation:

$$-\frac{dc}{dt} = \frac{v}{V} \cdot c \qquad (6)$$

where v = rate at which air enters or leaves the enclosure, ft^3/h;

$\forall$ = volume of enclosure, ft^3; and

c = concentration.

Separating the variables and solving eq. (6) yields

$$I = \frac{\ln(c_i/c_f)}{t} \tag{7}$$

Here c_i and c_f are the concentration of SF_6 for the initial and final bag samples, and t is the elapsed time between the bag samples.

5. WINTER HEATING SEASON MEASUREMENTS

5.1 Experimental Procedure

From January 4 to April 11, 1982, winter heating season measurements were carried out. During this 14-week measurement period, the thermostats of the test buildings were set for space heating at 68 $\pm$ 0.5°F (20 $\pm$ 0.3°C). The windows of the test buildings were maintained in a closed position, a constant internal load of 290 W was maintained within each building; and moisture was not released within the test buildings. During these measurements, the buildings typically did not float (i.e., heating energy as called for by the thermostat was supplied each hour of test).

For the winter heating season measurements, the entire floor surface of each test building was covered with 2-in.-thick (5.1 cm) polystyrene insulation in order to reduce the magnitude of a large heat-transfer phenomenon which could neither be accurately predicted from theory nor easily measured in the field. Winter heating season measurements of the preceeding year for which the floor slabs were uninsulated had to be essentially discarded because of the following floor heat-transfer phenomena:

1. floor edge loss was large and could not be accurately predicted;

2. about one-half of the solar beam radiation that penetrated south-facing windows and fell onto the slab floors was absorbed and permanently lost from the space; and

3. the supply registers of the heating plants directed heated air onto the floor slabs. A fraction of the heating energy content of this air was absorbed by the floor slabs and permanently lost from the space.

The daily electric load (Q_e) supplied to each test building was fitted to an equation[1/] of the form:

$$Q_e = K \cdot (T_i - T_o) + \beta \cdot H + D \qquad (8)$$

where $T_i - T_o$ = daily average inside-to-outside temperature difference, °F

H = daily-average solar radiation incident on a south-facing vertical surface, Btu/h·ft^2; and

K, β, and D = regression coefficients.

After the winter heating energy measurements were completed, the foregoing equation was used to normalize the weekly electric energy (Q_e) supplied to each test building to an indoor temperature of 68°F (20°C) and a solar vertical flux of 35.3 Btu/h·ft^2 (111 W/m^2). The temperature 68°F (20°C) was the intended indoor thermostat set temperature, and a daily-average solar vertical flux of 35.3 Btu/h·ft^2

1/ A correlation coefficient for the two independent variables (T_i-T_o) and H was computed to be 0.26 for the 98-day winter heating season data file. This value is not considered to be sufficiently large to cause multicollinearity problems for the regression eq. (8).

(111 W/m^2) was the average observed value for the 98-day measurement period.

5.2 Theory

During the winter heating season, when the test buildings did not float, the weekly heating load (Q_h) expressed in Btu/h for each test building may be predicted from the relation:

$$Q_h = K \cdot (T_b - T_o) \tag{9}$$

Here T_o is the average weekly outdoor temperature, and T_b is the outdoor balance-point temperature for the building. The coefficient (K) is the envelope heat-transfer coefficient which is computed from the relation:

$$K = \sum_{i=1}^{N} U_i \cdot A_i + \rho \cdot V \cdot I \cdot C_p \tag{10}$$

where U_i = thermal transmittance for i-th component, $Btu/h \cdot ft^2 \cdot °F$;
A_i = surface area for i-th component, ft^2;
ρ = density of air, lb/ft^3;
V = inside volume of building, ft^3;
I = rate of air infiltration, h^{-1}; and
C_p = specific heat of air, $Btu/lb \cdot °F$.

The outdoor balance point temperature (T_b) is determined from the relation:

$$T_b = T_i - \frac{Q_i + \beta \cdot H - U_f \cdot A_f \cdot (T_i - T_g)}{K} \tag{11}$$

where T_i = average-weekly indoor air temperature, °F;
Q_i = constant internal load for the test building, Btu/h;
β = solar loading coefficient, ft^2;
H = weekly-average solar radiation incident on a south-facing vertical surface, $Btu/h \cdot ft^2$;

U_f = thermal transmittance of floor, Btu/h•ft^2;

A_f = surface area of floor, ft^2; and

T_g = weekly-average temperature below the slab floors, °F.

The other symbols are as previously defined.

5.3 Results

The regression coefficients (K, β, and D) along with the residual standard deviation for the electric energy correlation (eq. 8) are summarized in Table 5.

Table 5

Summary of Regression Coefficients

Building	K Btu/h•°F	β ft^2	D Btu/h	Residual Standard Dev. Btu/h
1	87.2	8.17	359	± 241
2	167.0	14.8	266	± 287
3	79.0	7.08	632	± 194
4	146.6	14.7	337	± 312
5	82.2	6.33	500	± 211
6	87.0	6.80	709	± 272

The envelope heat-transfer coefficients determined from the regression analysis procedure are compared in Table 6 to corresponding predicted values determined from eq. (10). It can be seen that the predicted values agree within 12 percent or less of the corresponding measured values.

The solar loading coefficients (β) for the insulated buildings should be approximately equal to the product of the south-facing window

Table 6

Comparison of Measured and Predicted Envelope Heat-Transfer Coefficients, K

Building	K, Btu/h•°F Measured[1/]	K, Btu/h•°F Predicted[2/]	(P - M)/M[3/] % Diff
1	87.2	88.2	1.1
3	79.0	80.8	2.3
5	82.2	92.1[4/]	12.0
6	87.0	85.1	-2.0
2	167.0	180.4	+ 8.0
4	146.6	150.7[4/]	+ 2.8

1/ Determined from regression analysis.

2/ Determined from eq. (10).

3/ M and P denote measured and predicted values of envelope heat-transfer coefficients.

4/ Using wall heat-transfer coefficient from guarded-hot-box measurement.

1 Btu/h•°F = 0.527 W/K

1 ft^2 = 0.0929 m^2

1 Btu/h = 0.293 W

area (A_s) and the solar transmission coefficient for the window (τ), or,

$$\beta = A_s \cdot \tau \qquad \text{(for insulated buildings)} \qquad (12)$$

The surface area (A_s) for the south-facing windows is 21.9 ft^2 (2.03 m^2). An average value for the solar transmission coefficient (τ) was measured using a reflectometer and found to be 0.61. The predicted solar loading coefficient (β) is computed to be 13.4 ft^2 (1.24 m^2). The predicted β value is seen to be greater than the measured values given in Table 5 for the insulated buildings because the south-facing windows were shaded by the roof overhang during the last portion of the 98-day measurement period.

The regression coefficient (D) in eq. (8) is principally due to earth heat loss (q_e) through the floor slab which may be estimated from eq. (2). Taking (T_I - T_g) to be equal to the mean observed value for the six test buildings, an earth loss of 290 Btu/h (85.0 W) is computed. This value is the same order of magnitude as the regression coefficients (C).

Normalized weekly heating loads expressed in kW•h per day are compared to the steady-state theory in Figs. 3-8. In these figures, each data point represents one week of data and the straight line is the predicted heating load based on the steady-state theory. The agreement between measured values and corresponding values predicted from theory is good with the exception of Building No. 6. The small discrepancies between measured and predicted values for Building Nos. 2, 3, and 5 (Figs. 4, 5, and 7) are believed to be due to the inability to precisely predict the envelope heat-transfer coefficient (K) from known handbook heat-transfer properties for the building materials comprising the envelope. Since the heating loads were predicted with a steady-state model and since the steady-state model did not include the effect of thermal mass, it is concluded that thermal mass does not have a measure-

effect on the heating loads during the winter heating season. Furthermore, the observed differences for the masonry buildings were in different directions away from the steady-state correlations. If a thermal mass effect were present, then the observed differences for the masonry buildings would be in a consistent direction.

In the case of Building No. 6, a thermographic survey found perlite insulation to be missing under the windows and in a triangularly shaped region at the top of the north wall. When perlite insulation was poured into the top of the fully constructed wall, it apparently did not flow under the windows. For the triangularly shaped region, apparently perlite was lost from the wall, when the penetration was drilled for the air conditioning line. These insulation voids were accounted for in the calculation of the envelope heat-transfer coefficient by treating the insulation voids as a parallel heat flow path having a surface area of 34 ft^2 (10.4 m^2) and a thermal transmittance of 0.15 $Btu/h \cdot ft^2 \cdot °F$ (0.85 $W/m^2 \cdot K$).

When a measured value for the envelope heat-transfer is used in the analysis, the steady-state theory predicts a heating load correlation for Building No. 6 which lies below the measured data by a constant amount. This would suggest that there exists an unaccounted heat sink in Building No 6. High inside surface heat loss (stem wall effect) was observed at the base of the wall for Building No. 6. The results of a spot radiometer survey used to investigate this effect are given in Fig. 9. If the inside surface heat-loss rate is taken to be proportional to the observed temperature differences shown in Fig. 9, then considerably higher heat-loss rates exist at the base of the wall for Building No. 6 compared to the other insulated buildings. It was hypothesized that the earth heat loss through the base of the wall into the footing for Building No. 6 is the unaccounted heat sink which caused the measured heat-loss rates to be consistently higher than corresponding values predicted from the steady-state theory.

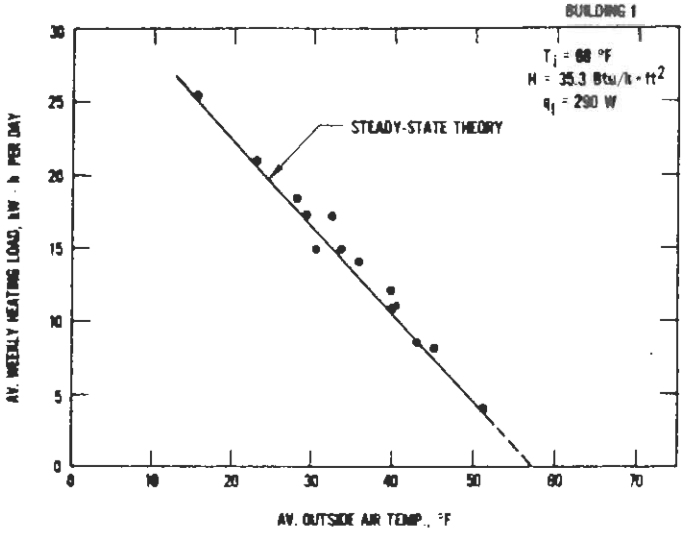

Fig. 3. Weekly heating load correlation for Building No. 1.

C = 5/9(F - 32)

1 Btu/h•ft^2 = 3.15 W/m^2

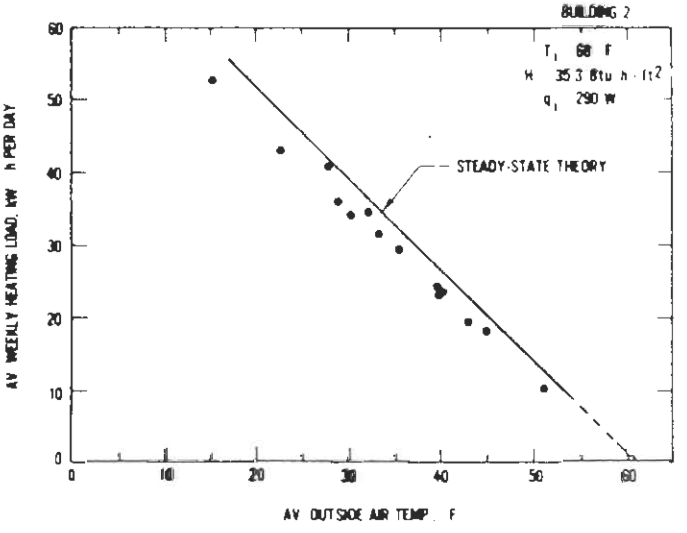

Fig. 4. Weekly heating load correlation for Building No. 2.

C = 5/9(F - 32)

1 Btu/h•ft^2 = 3.15 W/m^2

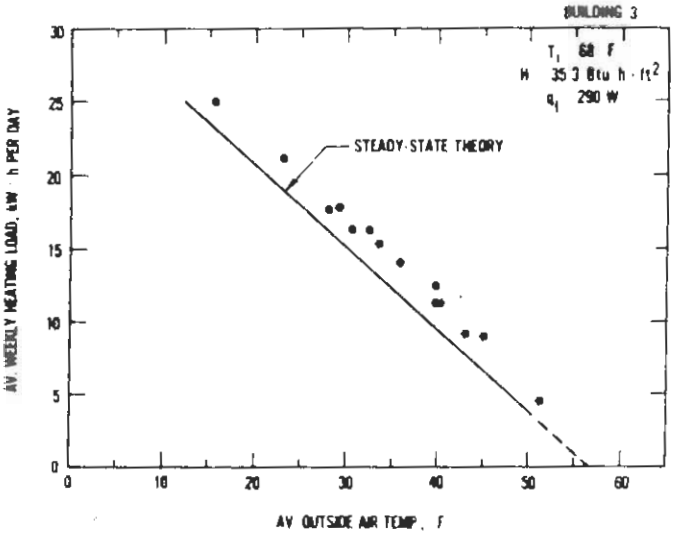

Fig. 5. Weekly heating load correlation for Building No. 3.

C = 5/9(F - 32)

1 Btu/h•ft^2 = 3.15 W/m^2

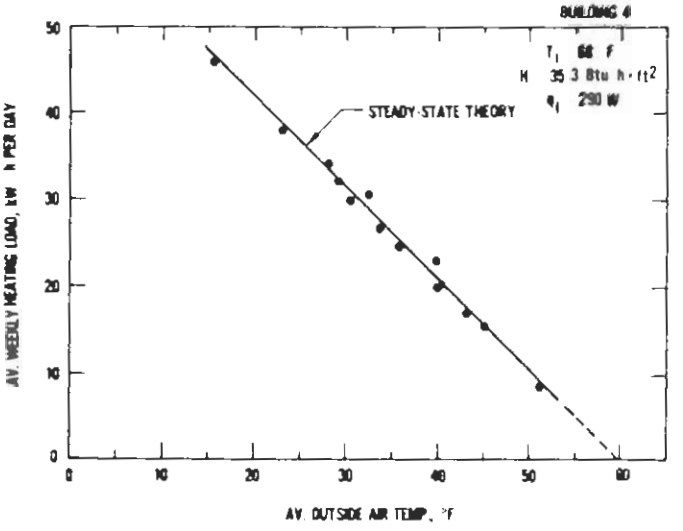

Fig. 6. Weekly heating load correlation for Building No. 4.

C = 5/9(F - 32)

1 Btu/h•ft^2 = 3.15 W/m^2

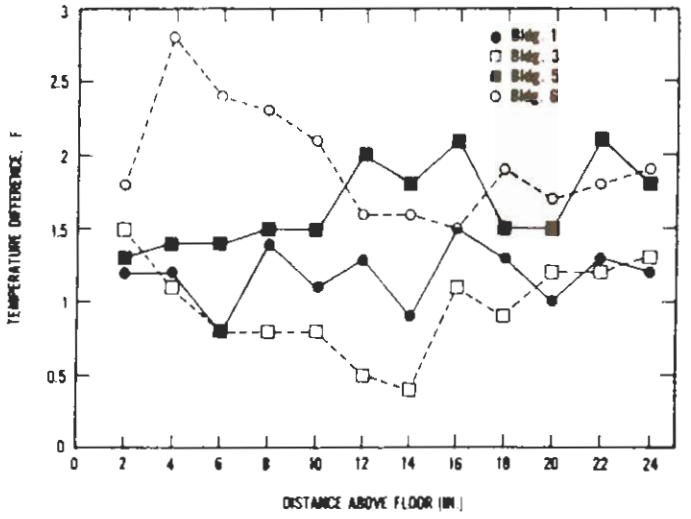

Fig. 9. Spot radiometer survey of stem wall effect in Building No. 6.

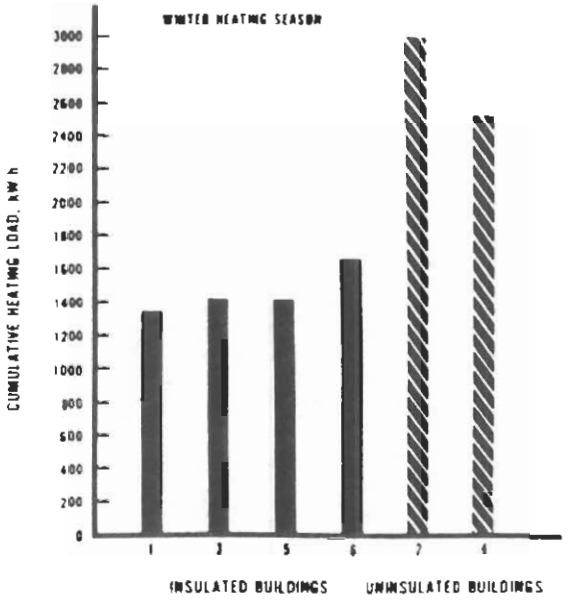

Fig. 10. Comparison of cumulative heating loads for the test buildings during the winter heating season.

Table 7

Summary of Daily Heating Loads (expressed in kW•h) for Test Buildings for Intermediate Heating Season

Period	T_o °F	T_{omin} °F	T_{omax} °F	H Btu/h•ft^2	Building 1	3	5	6	2	4
12-13 April, 82	50.6	44.8	59.6	43.	6.38	5.68	5.23	5.64	11.73	8.50
13-14 April, 82	56.2	37.1	76.7	54.	4.28	2.83	2.83	2.31	10.90	6.89
14-15 April, 82	50.0	36.7	76.1	52.	8.82	3.68	3.55	2.40	12.94	7.31
15-16 April, 82	55.2	41.3	67.1	28.	5.26	3.34	2.91	2.37	11.51	6.97
16-17 April, 82	65.6	60.0	75.0	29.	0.00	0.00	0.03	0.00	1.94	0.42
17-18 April, 82	63.1	46.7	81.6	31.	1.42	0.00	0.00	0.00	5.18	1.17
18-19 April, 82	52.9	37.2	66.6	53.	5.10	1.22	1.56	0.00	10.98	4.92
19-20 April, 82	58.6	46.9	71.2	43.	3.24	1.84	1.31	0.25	7.85	3.79
20-21 April, 82	59.2	54.2	65.3	70.	2.10	1.55	1.01	0.75	6.71	4.03
21-22 April, 82	50.1	38.3	62.2	43.	7.50	4.06	3.73	1.75	14.47	8.53
22-23 April, 82	47.2	31.1	58.2	48.	6.43	5.41	4.76	4.77	16.06	10.60
23-24 April, 82	55.4	43.4	66.3	48.	2.68	2.73	2.04	2.44	8.79	4.77
24-25 April, 82	59.4	41.1	73.8	47.	1.47	1.44	0.17	0.00	7.61	1.77
25-26 April, 82	65.3	54.2	78.0	29.	0.00	0.00	0.00	0.00	2.50	0.00
26-27 April, 82	59.6	55.4	64.5	8.0	0.58	1.54	0.00	0.00	5.91	2.45
27-28 April, 82	54.6	46.1	65.6	5.6	3.13	3.97	2.44	1.15	10.31	5.40
28-29 April, 82	49.2	35.9	60.6	35.	4.71	4.51	3.74	3.57	14.02	8.54
29-30 April, 82	52.2	37.1	64.0	43.	3.16	2.32	2.04	1.63	10.30	4.41
30 April-1 May, 82	57.0	40.3	69.9	39.	1.92	0.74	0.59	0.34	8.31	2.52
1-2 May, 82	61.8	45.3	75.2	29.	0.42	0.00	0.00	0.00	5.03	0.77
2-3 May, 82	61.3	44.1	73.6	39.	0.50	0.00	0.00	0.00	5.38	0.42
				TOTAL	69.10	46.86	37.94	29.37	188.43	94.18

C = 5/9(F - 32)

1 Btu/h•ft^2 = 3.152 x W/m^2

comparisons. Cumulative heating loads for the test buildings are compared in a bar graph given in Fig. 11.

Comparing Building Nos. 1 and 2, it is seen that the presence of thermal insulation in the wood-frame building reduced the cumulative heating load from 188.43 to 69.10 kW•h, or a reduction of 63 percent.

Comparing the insulated masonry buildings (Nos. 3 and 6) to the Uninsulated Masonry Building (No. 4), it is seen that the insulated masonry buildings consume less heating energy than the Uninsulated Masonry Building. The cumulative heating load for Building No. 6 (inside mass) is considerably less than that for Building No. 3 (outside mass). These results indicate that, for an intermediate heating season climate, where buildings typically float during warm day periods, optimum benefit of insulation and wall mass is achieved when the wall mass is located at the interior surface with the insulation positioned outside the wall mass.

Comparing the insulated masonry buildings (No. 3 and No. 6) to the Log Building (No. 5), it is seen that the Log Building is performing about midway between the two insulated masonry buildings.

Comparing Buildings Nos. 2 and 4, it is seen that the Uninsulated Masonry Building (No. 4) consumed 50 percent less heating energy than the Uninsulated Wood-Frame Building (No. 2).

During the intermediate heating season, the percent differences in cumulative heating loads between the wood-frame buildings and the comparable masonry buildings were large. However, the absolute value of these differences are very small compared with the cumulative loads measured during the winter heating season. This means that, for the climate in which the buildings were tested, wall mass has a small effect on the annual heating energy requirement.

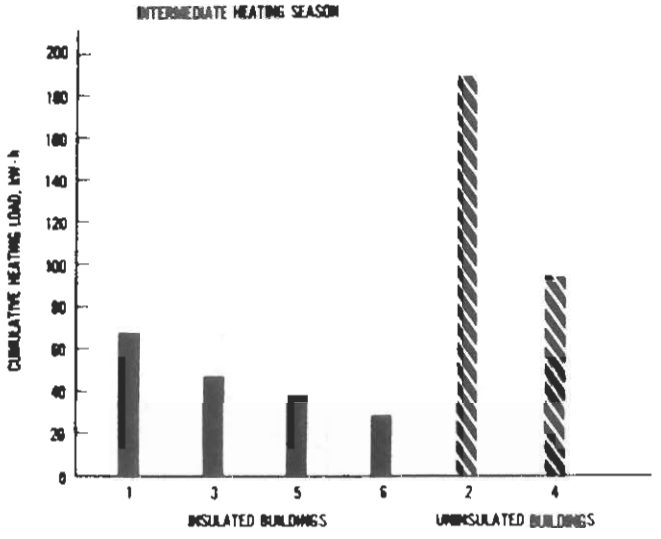

Fig. 11. Comparison of cumulative heating loads for the test buildings during the intermediate heating season.

The annual heating load for a building is given by the cumulative heating load during a fall intermediate heating season, a winter heating season, and a spring intermediate heating season. Since the cumulative heating loads which occur during the two intermediate heating seasons are very small in comparison to that which occurs during the winter heating season, the annual cumulative heating load can be estimated using a degree-day method. The insulated buildings had an envelope heat-transfer coefficient K=0.56 kW•h/°F and a balance point temperature T_b = 60.5°F. The number of heating degree days (DD) for Washington, DC at a balance point temperature of 60.5°F is 3290 degree days. The annual cumulative heating load is estimated to be:

$$q_h = K \cdot DD = 0.56\ (3290) = 1840\ kW \cdot h$$

During the intermediate heating season, the Insulated Masonry Building with outside wall mass (No. 3) consumed 22 kW•h less than the Insulated Wood-Frame Building (No. 1). If it is assumed that this figure constitutes the heating energy savings which would occur during both fall and spring intermediate heating seasons, then the annual percent savings due to wall mass in Building No. 3 is computed to be

$$\% \text{ savings} = \frac{22 + 22}{1840} = 2.4\%$$

It is interesting to note that this amount is close to the value of 2.3 percent obtained by Goodwin and Catani [3] using a computer simulation of a low-rise residential building located in Washington, DC.

In comparing the cumulative heating loads for the insulated buildings during the intermediate heating season, it should be kept in mind that the steady-state heat-transfer characteristics for these buildings as determined by the winter heating measurements were not exactly identical (i.e., the cumulative heating load for the Insulated Masonry Building with inside wall mass (No. 6) was higher than that for the other insulated buildings due to anomalies in its building envelope). If these thermal anomalies had not been present in the

Insulated Masonry Building with inside wall mass (No. 6), then it would have had even a lower cumulative heating load during the intermediate heating season.

Likewise, in comparing the cumulative heating loads for the uninsulated buildings during the intermediate heating season, it should be kept in mind that the steady-state heat-transfer characteristics for these buildings as determined by the winter heating measurements were not exactly identical (i.e., the cumulative heating loads for the Uninsulated Masonry Building (No. 4) was lower than that for the Uninsulated Wood-Frame Building (No.2) due to the fact that the thermal resistance of the walls as constructed deviated from their intended design values). If the envelopes of these buildings have had identical envelope heat-transfer characteristics, then the observed differences between these buildings during the intermediate heating season would have been smaller.

7. SUMMER COOLING SEASONS MEASUREMENTS

7.1 Experimental Procedure

From July 6 to September 21, 1981, summer cooling season measurements were carried out. During this 11-week period, the thermostats of the test buildings were set for space cooling at 76 $\pm$ 0.5°F (24 $\pm$ 0.3°C). The windows of the test buildings were maintained in a closed position; a constant internal load of 290 W was maintained within each building; and moisture was not released within the test buildings. During these measurements, the buildings typically floated during cool night periods (i.e., no mechanical cooling was provided at night). Space cooling was provided during warm day periods. For these measurements, polystyrene insulation was not installed over the top surface of the slab floors.

7.2 Results

The cumulative sensible cooling loads consumed by the test buildings are summarized in Table 8. In this table, the insulated and uninsulated buildings again have been grouped together to facilitate comparisons. The cumulative sensible cooling loads are compared in a bar graph given in Fig. 12.

Comparing Building Nos. 1 and 2, it is seen that the presence of thermal insulation in the wood-frame building reduced the cumulative sensible cooling load from 214.1×10^4 Btu (2.26×10^9 J) to 133.2×10^4 Btu (1.41×10^9 J), or a reduction of 38 percent.

Comparing the Insulated Masonry Building with outside wall mass (No. 3) to the Uninsulated Masonry Building (No. 4), it is seen that wall insulation appears to have only a small effect when it is placed inside the wall mass. On the other hand, comparing the Insulated Masonry Building with inside wall mass (No. 6) to the Uninsulated Masonry Building (No. 4), it is seen that wall insulation appears to have a very beneficial effect when it is placed outside the wall mass. These results indicate that, in a summer cooling season during which buildings typically float during cool night periods, optimum benefit of insulation and wall mass is achieved when the wall mass is located at the interior surface with the insulation positioned outside the wall mass.

Comparing the Log Building (No. 5) to the Insulated Masonry Buildings (Nos. 3 and 6), it would appear that the Log Building is performing midway between the two insulated masonry buildings. It is hypothesized that the stem wall effect in Building No. 6 is providing a constant heat loss from this building to the earth, thereby causing Building No. 6 to have smaller cumulative cooling loads. If the stem wall effect were not present, then Building No. 6 perhaps would perform more like Building No. 5.

Table 8

Summary of Cumulative Sensible Cooling Loads (10^4 Btu) for summer cooling season

Period	Building 1	3	5	6	2	4
July 6-July 13	22.8	21.8	17.7	16.8	34.5	23.5
July 13-July 20	19.7	17.7	15.1	12.8	29.0	19.4
July 20-July 27	12.3	11.8	9.6	8.3	19.3	11.7
July 27-Aug 3	14.4	14.4	10.5	9.2	23.0	13.5
Aug 3-Aug 10	14.3	14.0	11.3	10.7	21.8	15.0
Aug 10-Aug 17	15.9	15.3	12.5	11.2	25.3	17.2
Aug 17-Aug 24	8.8	5.7	3.0	2.3	13.1	5.8
Aug 24-Aug 31	10.3	11.5	9.0	6.0	19.2	11.2
Aug 31-Sep 8	5.7	6.8	5.6	4.0	11.6	5.0
Sep 8- Sep 14	6.2	5.3	4.0	3.5	12.0	5.5
Sep 14-Sep 21	2.8	3.0	2.5	3.0	5.3	3.2
Totals	133.2	127.3	100.8	87.8	214.1	131.0

1 Btu = 1.056×10^3 J

Another interesting comparison may be made between Building Nos. 1 and 4. The Uninsulated Masonry Building (No. 4) is seen to consume 2 percent less cumulative sensible cooling load than the Insulated Wood-Frame Building (No. 1). The results indicate that masonry buildings constructed in similar climates perhaps may not need to be insulated when the purpose of the insulation is to reduce cooling loads.

In considering the percentage difference figures presented in this section, it should be kept in mind that the uncertainty in the sensible cooling load measurement is about $\pm$ 6 percent. When two buildings are compared, it is possible that one building was measured 6 percent too high and the other 6 percent too low. Therefore, differences in cumulative cooling loads should be considered to be uncertain by 12 percent. Therefore, observed differences of less than 12 percent may not be real.

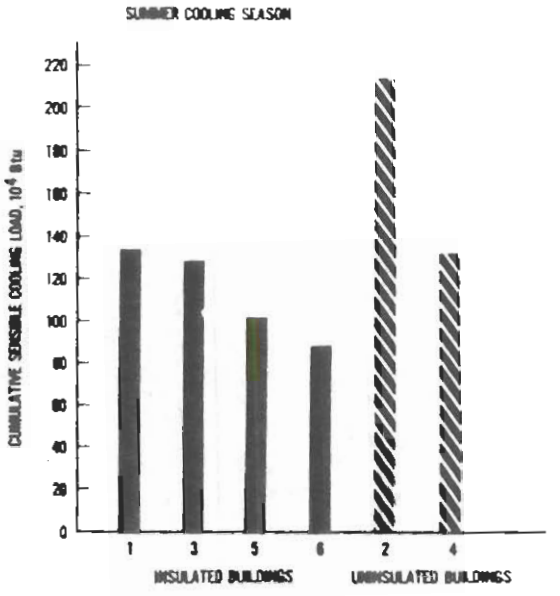

Fig. 12. Comparison of cumulative cooling loads for test during during the summer cooling season.

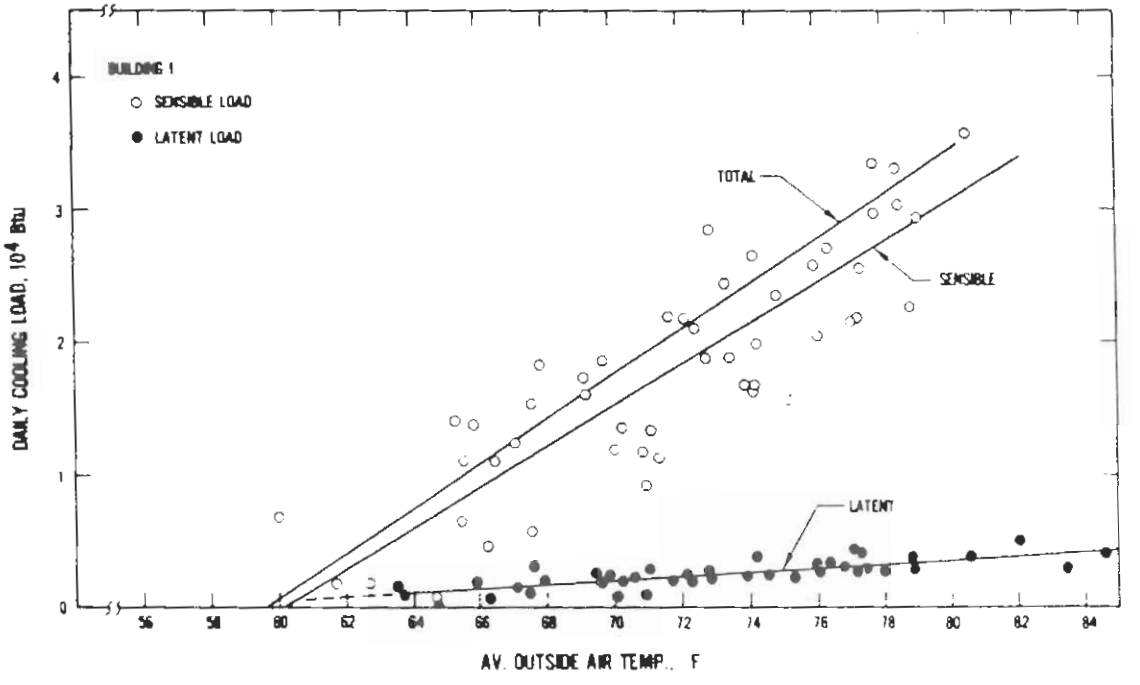

Fig. 13. Cooling load correlations for Building No. 1.

1 Btu = 1.056 x 10^3 J

An attempt was made to correlate daily cooling loads with the daily average outdoor temperature. Such a correlation is shown for the Insulated Wood-Frame Building (No. 1) in Fig. 13. It is seen that considerable scatter is present in the sensible load data, suggesting that other factors (such as incident solar radiation and diurnal temperature swing) are affecting the results. In order to examine the trend of the data, both the sensible and latent load data were fitted to a best-fit straight line using a least-squares procedure. The total cooling load line was obtained by summing the sensible and latent load correlations.

Similar cooling load correlations were obtained for the other test buildings. The total cooling load correlations for the insulated buildings are compared in Fig. 14 and for the uninsulated buildings in Fig. 15. These total cooling load correlations obtained from scatter plots rank the buildings in the same order as obtained from the cumulative sensible load analysis presented at the beginning of the section.

8. CAUTIONS

The effects of thermal wall mass has been shown to be climate dependent [1, 2, 3, and 5]. Therefore, the test results of the present study should not be directly extended to other climates.

Perhaps equally important is the fact that the test results should not be extended to a real house situation for the following reasons:

1) The test buildings were one-room test cells which did not contain interior partition walls and interior furnishings. The addition of interior partition walls and interior furnishings would have added considerable interior mass which would have affected the observed results; and

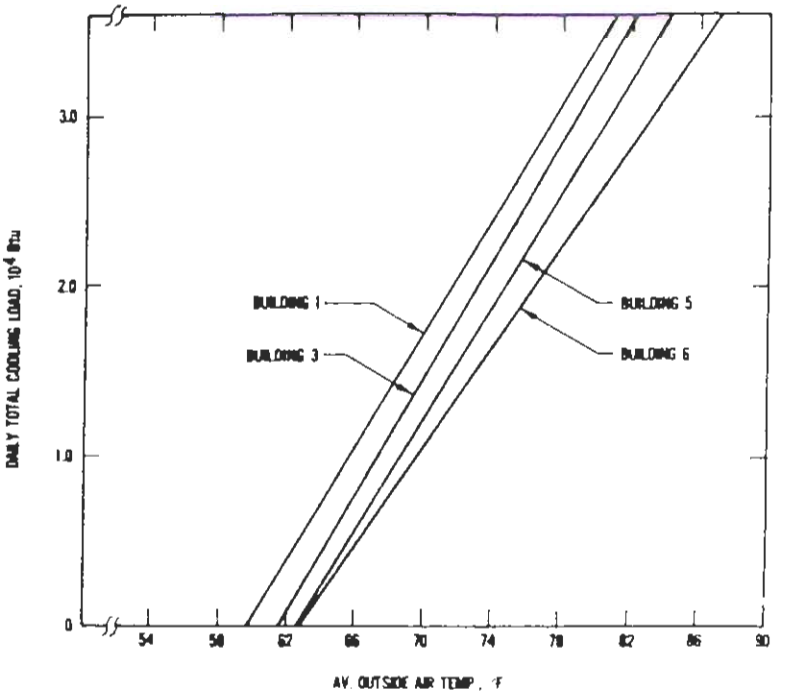

Fig. 14. Comparison of total cooling load correlations for insulated buildings.

1 Btu = 1.056 x 10^3 J

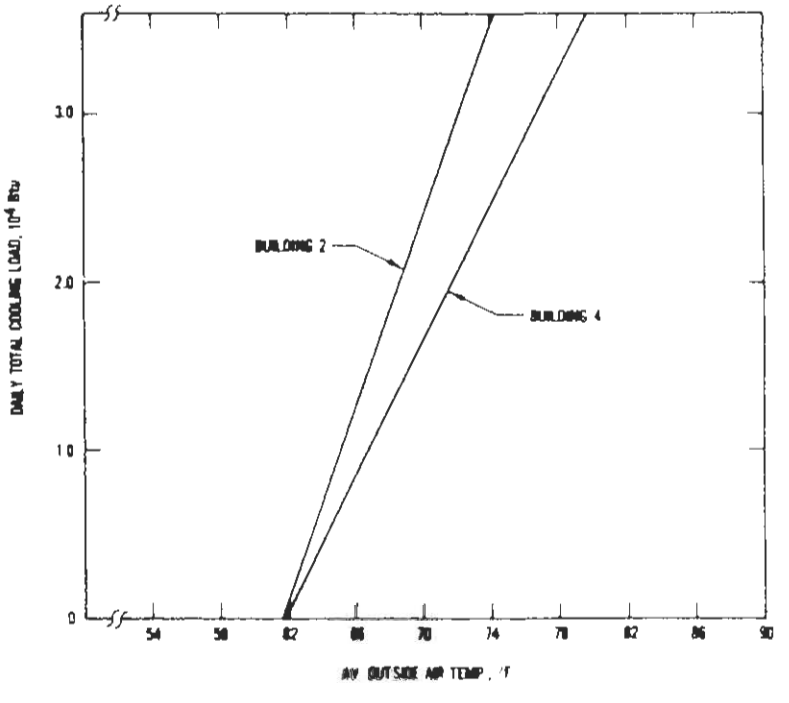

Fig. 15. Comparison of total cooling load correlations for uninsulated buildings.

1 Btu = 1.056 x 10^3 J

2) Heat transmission through the walls of the test buildings was a larger part of the overall envelope heat transfer compared to a typical house due to high thermal resistance in other components of the building envelopes (i.e., the ceilings contained R-34 (R-6.0 $m^2 \cdot K/W$) glass-fiber insulation, the windows contained triple glazing, the floor slabs were insulaced over the top with R-11.2 (R-1.97 $m^2 \cdot K/W$) polystyrene insulation, and the air infiltration rates were quite small).

9. SUMMARY AND CONCLUSIONS

Six test buildings were extensively instrumented for measuring heating and cooling loads, wall heat transmission, and indoor temperature and humidity. During these measurements, the effect of wall mass on the heating and cooling loads was observed. These buildings were exposed to a winter heating season, an intermediate heating season, and a summer cooling season. For these measurements, the windows of the test buildings were maintained in a closed position; a constant internal load of 290 W within each building was maintained; and the thermostats were set at a fixed setpoints for either space heating or space cooling.

The six 20 x 20 ft (6.1 x 6.1 m) one-room test buildings were constructed at Gaithersburg, Maryland. These buildings had the same floor plan and orientation. They were identical, except for the wall construction, which was as follows: No. 1 insulated lightweight wood frame; No. 2 uninsulated lightweight wood frame; No. 3 insulated masonry (outside mass); No. 4 uninsulated masonry; No. 5 log; and No. 6 insulated masonry (inside mass). Building Nos. (1, 3, 5, and 6) and Buildings Nos. (2 and 4) were designed to have walls of approximately the same steady-state thermal resistance. With the exception of Building No. 6, an effort was made to make the construction representative of current construction practices.

During the winter heating season, when the buildings typically did not float (i.e., some heating energy was supplied each hour), measured weekly heating loads for the buildings were closely predicted with a steady-state heat-transfer model, except for Building No. 6. In the case of Building No. 6, the observed difference between the steady-state theory and the measured heating loads was due to an unaccounted internal heat sink which was believed to be caused by heat conduction through the base of the wall into the footing and earth. Small differences were observed between the steady-state theory and measured heating loads for Building Nos. 2, 3, and 5. These differences were believed to be due to the inability to predict precisely the envelope heat-transfer coefficients. Furthermore, obaerved differences for the masonry buildings were in different directions away from the steady-state correlations. If a thermal mass effect were present, then the observed differences for the masonry buildings would be in a consistent direction. Since the steady-state theory does not account for the effect of thermal mass, it was concluded that no measured thermal mass effect was observed during the winter heating season.

During the intermediate heating season, when the test buildings often floated during warm day periods, a significant thermal mass effect was observed. Residential buildings with masonry walls were found to consume less heating energy than comparable buildings having wood-frame walls of the same steady-state thermal resistance. Wall mass was found to be considerably more effective when it was placed inside the wall insulation as opposed to outside the wall insulation. The Log Building (No. 5) performed about midway between the two insulated masonry buildings. During the intermediate heating season, the percent differences in cumulative heating loads between the wood-frame buildings and comparable masonry buildings having equivalent steady-state thermal resistance in the walls were large. However, the absolute values of these differences were shown to be small compared with the annual cumulative heating loads. For the climate in which the buildings were tested, it was shown that the Insulated Masonry Buildings with

outside wall mass (No. 3) had annual heating requirements which were only slightly less than for the comparable Insulated Wood-frame Building (No. 1).

During the summer cooling season, when the test buildings often floated during cool night periods, a significant mass effect was also observed. Residential buildings with masonry walls were found to have smaller cumulative cooling loads than comparable buildings having wood-frame walls of the same steady-state thermal resistance. Wall mass was found to be considerably more effective when it was placed inside the wall insulation as opposed to outside the wall insulation. The Log Building (No. 5) performed midway between the two insulated masonry buildings.

ACKNOWLEDGMENT

The authors would like to thank Mary Ramsburg for the excellent job of preparing this manuscript for publication.

REFERENCES

1. S. R. Petersen, K. A. Barnes, B. A. Perry, "Determining Cost-effective Insulation Levels for Masonry and Wood-Frame Walls in New Single-Family Housing," NBS Building Science Series 134, National Bureau of Standards, August 1981.

2. William Rudoy and Richard S. Dougall, "Effects of the Thermal Mass on Heating and Cooling Load in Residences," ASHRAE Transactions, Vol. 85, Part 1, pp. 903-917, 1979.

3. Stanley E. Goodwin and Mario J. Catani, "The Effects of Mass on Heating and Cooling Loads and on Insulation Requirements of Buildings in Different Climates," ASHRAE Transactions, Vol. 85, Part 1, pp. 869-884, 1979.

4. G. P. Mitalas, "Relation Between Thermal Resistance and Heat Storage in Building Enclosures," Building Research Note No. 126, Division of Building Research, National Research Council of Canada, January 1978.

5. C. Curtis, B. Anderson, R. Kammerud, W. Place, and K. Whitley, "Thermal Mass: Its Role in Residential Construction," International Conference on Energy Use Management, Los Angeles, October 1979.

APPENDIX

HEAT-TRANSFER PROPERTIES OF BUILDING COMPONENTS

Property	ℓ in.	K Btu·in./h·ft²·°F	ρ lb/ft³	C_p Btu/lb·°F	R ft²·h·°F/Btu
1. Properties of Walls of Test Buildings					
No. 1 Insulated Lightweight Wood Frame					
Component					
Gypsum Board	0.5	1.11	50.0	0.26	0.45
2 x 4 studs placed 16 in. o.c.	3.625	0.80	32.0	0.33	4.53
R-11 Blanket Insulation between Studs	3.625	0.33	2.0	0.20	11.00
Exterior Plywood	0.625	0.80	45.0	0.29	0.78
Note: Framing = 20%					
No. 2 Uninsulated Lightweight Wood Frame					
Same as No. 1, except R-11 Blanket Insulation is replaced with R-1.0 Air Space.					
No. 3 Insulated Masonry (Outside Mass)					
Component					
Gypsum Board	0.5	1.11	50.0	0.26	0.45
Polystyrene Insulation	2.0	.18	2.7	0.29	11.20
Furring Strips placed 24 in. o.c.	2.0	0.80	32.0	0.33	2.50
Air Space	0.25	--	--	--	0.69
Concrete Block at 105 lb/ft³	4.0	3.60	61.0	0.20	1.11
Face Brick	3.5	4.38	125.0	0.22	0.80
Note: Framing = 10%					
No. 4 Uninsulated Masonry					
Component					
Gypsum Board	0.5	1.11	50.0	0.26	0.45
Air Space	0.75	--	--	--	0.94
Furring Strips placed 16 in. o.c.	0.75	0.80	32.0	0.33	0.94
Concrete Block at 105 lb/ft³	8.00	5.03	61.0	0.20	1.59
Note: Framing = 7.6%					
No. 5 Log					
Component					
Square Lodge-pole Pine Log (9% Moisture Content)	7	0.80	25.9	0.39	8.75
No. 6 Insulated Masonry (Inside Mass)					
Component					
Plaster	0.50	1.56	45.0	0.20	.32
Concrete Block at 105 lb/ft³	8.00	5.03	61.0	0.20	1.59
Perlite Insulation	3.50	0.37	8.5	0.26	9.45
Face Brick	3.5	4.38	125.0	0.22	0.80
2. Properties of Ceilings					
Component					
Gypsum Board	0.5	1.11	50.0	0.26	0.45
2 x 4 stud	3.625	0.80	32.0	0.33	4.53
Glass-fiber Insulation	11.0	0.33	2.0	0.20	34.1
Note: Framing Fraction = 6.3%					
3. Floor Properties					
Component					
Polystyrene Insulation[1/]	2.0	.18	2.7	0.29	11.20
Concrete Slab	4.0	9.6	150.	0.20	.42
Gravel[2/]	4.0	6.0	120.	0.20	.67
Earth	12.0	6.0	120.	0.20	2.00

1/ Polystyrene was installed during the measurements for the winter heating season and the intermediate heating season, but not for the summer cooling season.

2/ Assumed to be the same as earth.

1 in. = 2.54 cm
1 Btu·in./h·ft²·°F = 0.144 W/m·K
1 lb/ft³ = 16.0 kg/m³
1 Btu/lb·°F = 4190 J/kg·K
1 ft²·h·°F/Btu = 0.176 m²·K/W